ISIJ International, Vol. 43 (2003), No. 9, pp. 1348–1355

Wetting of Solid Al_2O_3 with Molten $CaO–Al_2O_3–SiO_2$

Ja-Yong CHOI and Hae-Geon LEE[1)]

Formerly Graduate Student, Department of Materials Science and Engineering, Pohang University of Science and Technology, now at the STS Research Group, Technical Research Laboratories, POSCO, Pohang, 790-785, Korea.
1) Department of Materials Science and Engineering, Pohang University of Science and Technology (POSTECH), Pohang, 790-784, Korea. E-mail: hglee@postech.ac.kr

(*Received on January 6, 2003; accepted in final form on March 25, 2003*)

The wetting behavior of solid Al_2O_3 with molten $CaO–Al_2O_3–SiO_2$ was investigated at 1 873 K using the sessile drop method. A new model was developed to represent the time dependence of the contact angle, *i.e.*, the spreading behavior of a liquid drop on a solid substrate. The model takes into consideration chemical interactions which continually take place at the interface between the solid Al_2O_3 and molten $CaO–Al_2O_3–SiO_2$. By applying the model to the experimental results of the present study the equilibrium contact angle between the liquid slag and solid alumina was determined for a number of different slag compositions, and an iso-contact angle diagram was constructed. The equilibrium contact angle was greatly affected by the slag composition, and it was found that the interfacial tension was the major factor governing the equilibrium contact angle. In the region of low SiO_2 content, the slag with higher CaO content exhibits a smaller contact angle, *i.e.*, better wettability with alumina. For slag with a given CaO/SiO_2 ratio, an increase in Al_2O_3 results in a corresponding increase in the contact angle, *i.e.*, decrease in wettability. For a given CaO/Al_2O_3 ratio, the variation of the contact angle with SiO_2 content shows a minimum. The contact angle decreases by increasing the surface roughness of the alumina substrate.

KEY WORDS: contact angle; equilibrium; spreading; rate; $CaO–Al_2O_3–SiO_2$ slag; alumina; Al_2O_3; substrate; interfacial tension.

1. Introduction

Non-metallic inclusions form mainly by deoxidation in the steelmaking process. Their presence in steel causes a number of problems in steelmaking processes and with steel products, and consequently they must be removed as much as possible before casting. In general the density of inclusions are lower than that of liquid steel, and hence they tend to float up toward the metal surface which is covered by molten slag. In most steel refining processes liquid steel is stirred and hence inclusions move along with the steel flow. In the vicinity of the metal/slag interface the metal tends to flow parallel to the interface, and inclusions, particularly small ones, have a tendency of following the steel flow. For efficient removal of inclusions it is desired for inclusions to attach themselves firmly to the slag phase when they reach the interface and hence not to follow the steel flow, but quickly dissolve into the slag. Any inclusions not firmly grasped by the slag will be susceptible to re-entrapment into the flowing steel stream. This will lead to a low efficiency of inclusion removal. In order to produce a clean steel, therefore, slag at the refining stage should satisfy two basic requirements, *i.e.*, to exhibit high wettability with inclusions and to offer high dissolution rate of inclusions into it. In the present study, the rate of spreading of slags on an alumina substrate, that is, the wettability and the rate of wetting, was measured experimentally, and a theoretical model was developed to quantitatively describe the spreading behavior and to determine the equilibrium contact angle.

2. Experimental

The alumina substrate was prepared with the sintered Al_2O_3 ($\geq$99.8 %) (22×10^{-3} m$\times20\times10^{-3}$ m$\times3\times10^{-3}$ m). All substrates were polished to keep the surface roughness identical. The roughness was measured by using a non-contacting surface roughness measuring apparatus (Rodenstock RM600®) and the mean center-line roughness (R_a) was measured to be 0.553μm. Some substrates were prepared with different surface roughness in order to investigate the effect of the surface roughness of alumina substrate.

Slag samples for the measurement of wetting behavior were prepared by mixing master slags of an appropriate ratio to weigh a total of 0.3×10^{-3} kg. Each sample was pressed to form a small pellet. The master slags were prepared by mixing oxides (Al_2O_3, SiO_2, CaO and MgO) of reagent grade at an appropriate proportion and melted in a graphite crucible using a high frequency induction furnace and the slags were then quenched, ground into powder, and decarburized by heating under the atmosphere at 1 273 K for 12 h. The composition of the master slags was confirmed by XRF analysis. The slag compositions investigated in the present study are given in **Fig. 1** and also in **Table 1**.

The apparatus employed to measure the change of the

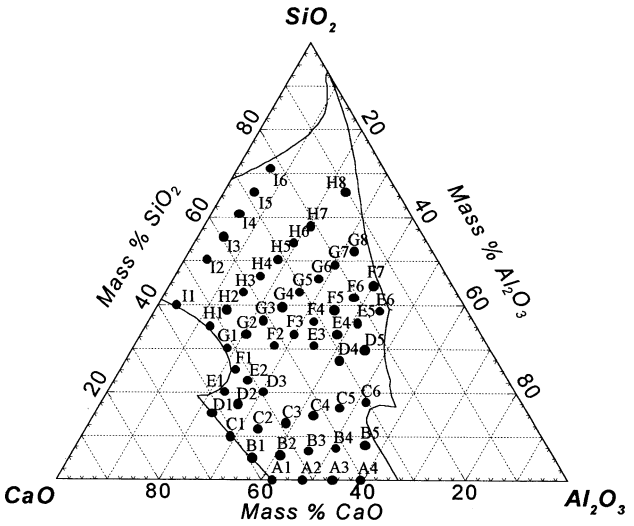

Fig. 1. Investigated slag compositions.

wetting angle over time is schematically shown in **Fig. 2**. An alumina substrate (7) was positioned horizontally in the induction furnace (15 kW–20 kHz). A slag pellet was held in a graphite slag holder (5) with a small hole (2×10^{-3} m in diameter) at the bottom. The furnace including the substrate and the slag holder with the slag pellet was heated at a rate of 100 K/min up to 1 873 K under an inert atmosphere by flowing purified argon gas. The system was held isothermally for 10 min at 1 873 K to ensure complete melting of the slag sample. The molten slag was then slowly squeezed out of the slag holder through the hole at the bottom by pressurizing the tube (3) with a bellow connected to the slag holder.

From the instant when the molten slag drop touched the alumina substrate, the change of the shape, *i.e.*, the wetting behavior, was continually recorded by using a digital video camera running at 30 frames/sec. Using image capturing software (MIRO DC-20 PLUS®), and image digitizing software (WINDIG®), the change in the height and width of the drop with time was precisely measured.

Table 1. Slag compositions and spreading parameters.

Run No.	Slag compositions (mass %)			Spreading parameters			
	CaO	SiO_2	Al_2O_3	$\cos\theta^{o}_{e,app}$	$\cos\theta^{\infty}_{e,app}$	k	m
A1	57.7	0.0	42.3	0.729	0.953	0.099	1.748
A2	51.9	0.0	48.1	0.658	0.901	0.079	2.354
A3	46.2	0.0	53.8	0.519	0.787	0.130	4.855
A4	40.4	0.0	59.6	0.478	1.000	0.051	2.714
B1	59.4	5.0	35.6	0.723	0.935	0.113	2.772
B2	53.5	5.7	40.8	0.687	0.858	0.107	5.798
B3	47.5	6.5	46.0	0.572	0.798	0.093	2.805
B4	41.6	7.2	51.2	0.546	0.815	0.119	4.304
B5	35.6	7.9	56.4	0.531	0.774	0.121	3.072
C1	60.8	10.0	29.2	0.690	0.924	0.092	5.728
C2	54.7	11.6	33.7	0.637	0.878	0.105	2.775
C3	48.6	13.1	38.3	0.575	0.861	0.087	3.073
C4	42.6	14.7	42.8	0.567	0.875	0.101	3.422
C5	36.5	16.2	47.3	0.537	0.853	0.148	3.987
C6	30.4	17.8	51.8	0.534	0.855	0.098	2.445
D1	62.0	15.0	23.0	0.640	0.917	0.116	6.863
D2	55.8	17.4	26.8	0.598	0.882	0.134	3.372
D3	49.6	19.9	30.5	0.631	0.909	0.090	3.212
D4	31.0	27.2	41.8	0.602	0.921	0.089	1.602
D5	24.8	29.7	45.5	0.445	0.913	0.160	3.918
E1	57.0	20.0	23.0	0.621	0.882	0.099	1.902
E2	51.3	22.6	26.1	0.623	0.889	0.113	2.483
E3	34.2	30.6	35.2	0.645	0.930	0.086	1.503
E4	28.5	33.2	38.3	0.620	0.948	0.051	0.975
E5	22.8	35.9	41.3	0.536	0.965	0.030	0.734
E6	17.1	38.5	44.4	0.395	0.894	0.115	4.757
F1	52.5	25.0	22.6	0.661	0.902	0.090	1.453
F2	42.0	30.5	27.5	0.677	0.935	0.118	1.031
F3	36.7	33.3	30.0	0.710	0.947	0.097	1.902
F4	31.5	36.0	32.5	0.710	0.977	0.065	0.990
F5	26.2	38.8	35.0	0.703	0.971	3.013	0.601
F6	21.0	41.5	37.5	0.503	1.000	0.021	0.653
F7	15.7	44.3	40.0	0.427	0.915	0.108	2.601
G1	51.5	30.0	18.5	0.676	0.916	0.103	2.275
G2	46.3	33.2	20.5	0.742	0.944	0.130	4.523
G3	41.2	36.4	22.5	0.721	0.947	0.151	4.731
G4	36.0	39.5	24.4	0.724	0.977	0.072	1.381
G5	30.9	42.7	26.4	0.728	0.966	0.308	4.560
G6	25.7	45.9	28.4	0.494	0.946	3.000	0.506
G7	20.6	49.1	30.3	0.470	1.000	2.977	0.506
G8	15.4	52.3	32.3	0.358	1.000	1.367	0.275
H1	52.4	35.0	12.7	0.688	0.945	0.160	4.254
H2	47.1	38.8	14.0	0.744	0.954	0.095	2.826
H3	41.9	42.7	15.4	0.738	0.957	0.114	1.262
H4	36.6	46.5	16.8	0.736	0.980	0.082	1.392
H5	31.4	50.4	18.2	0.773	1.000	0.047	0.935
H6	26.2	54.2	19.6	0.552	0.942	2.913	0.488
H7	20.9	58.1	21.0	0.424	0.918	2.284	0.373
H8	10.5	65.8	23.8	0.272	1.000	1.000	0.142
I1	56.3	40.0	3.7	0.732	0.936	0.092	1.190
I2	45.1	50.3	4.6	0.795	0.998	0.063	2.087
I3	39.4	55.5	5.1	0.862	1.000	0.053	1.307
I4	33.8	60.7	5.5	0.783	0.961	0.190	5.661
I5	28.2	65.8	6.0	0.592	0.909	1.878	0.533
I6	22.5	71.0	6.5	0.490	0.970	1.453	0.267

3. Results

3.1. Spreading Behavior

A typical example of the spreading and wetting behavior of a liquid slag drop on an alumina substrate is shown in **Fig. 3**. It is seen that the liquid drop spreads out on the substrate with time. In the present study the moment at which the slag drop forms the right angle with the substrate is taken as the zero time. The experimental results of the spreading behavior are shown in **Fig. 4**. It is obvious that the spreading continues to proceed until the contact angle has reached the limiting value which is the equilibrium contact angle. General observations from the figure can be summarized as follows:

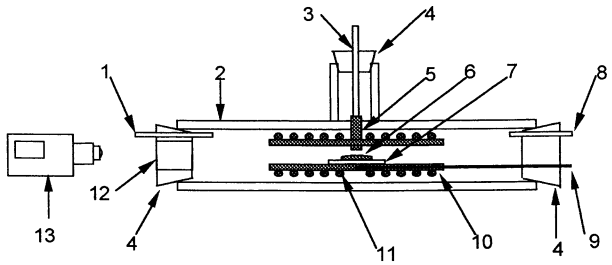

Fig. 2. Experimental apparatus.

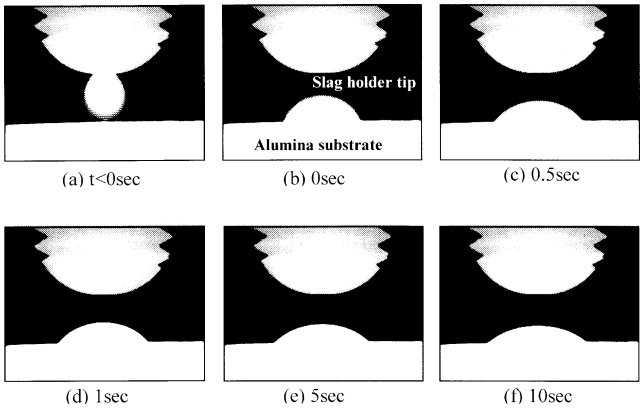

Fig. 3. Spreading behavior of slag on an alumina substrate. (slag: A2, *T*: 1 873 K)

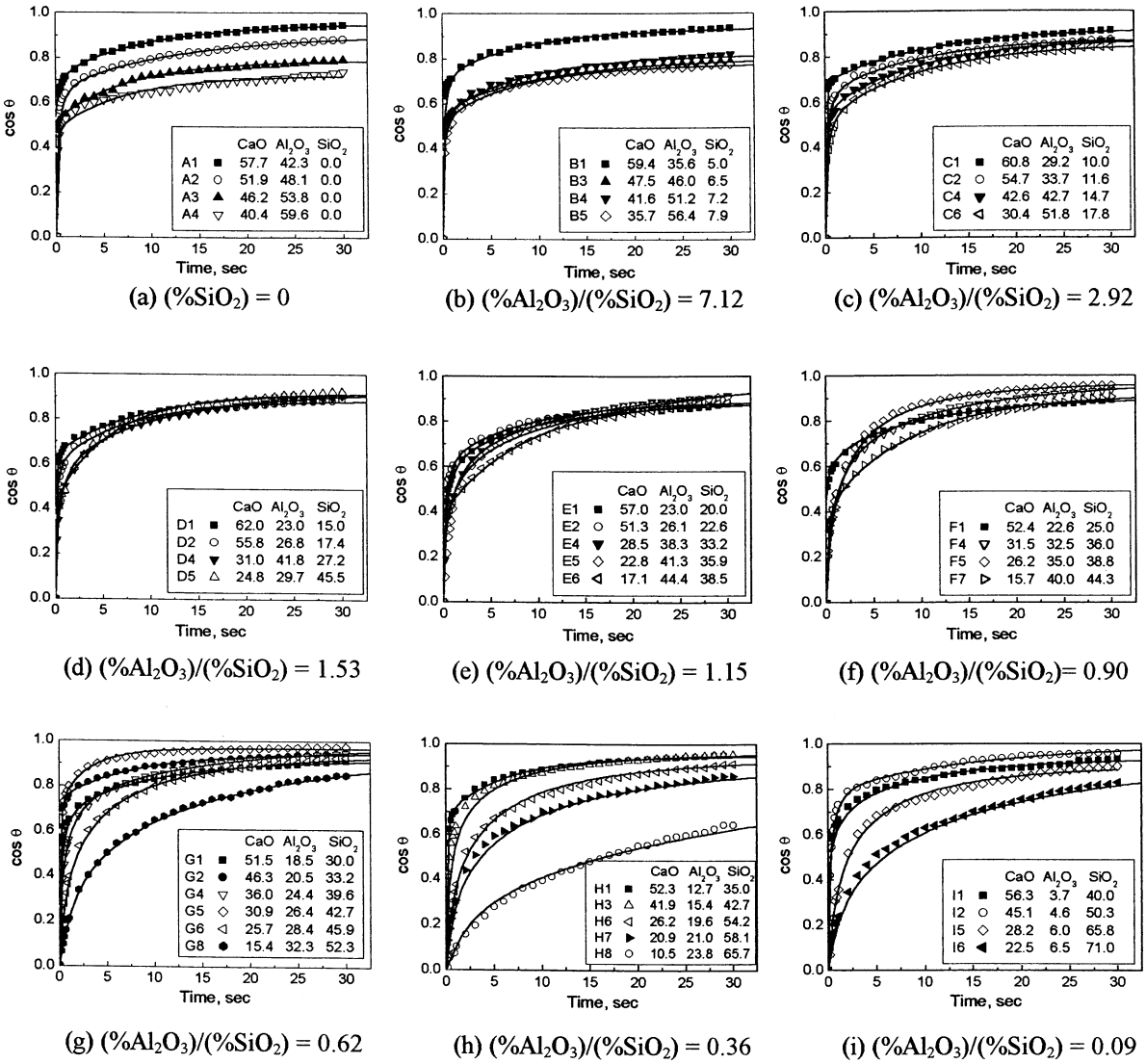

Fig. 4. Spreading behavior of slag of different compositions (mass%) on Al_2O_3 substrate at 1 873 K.

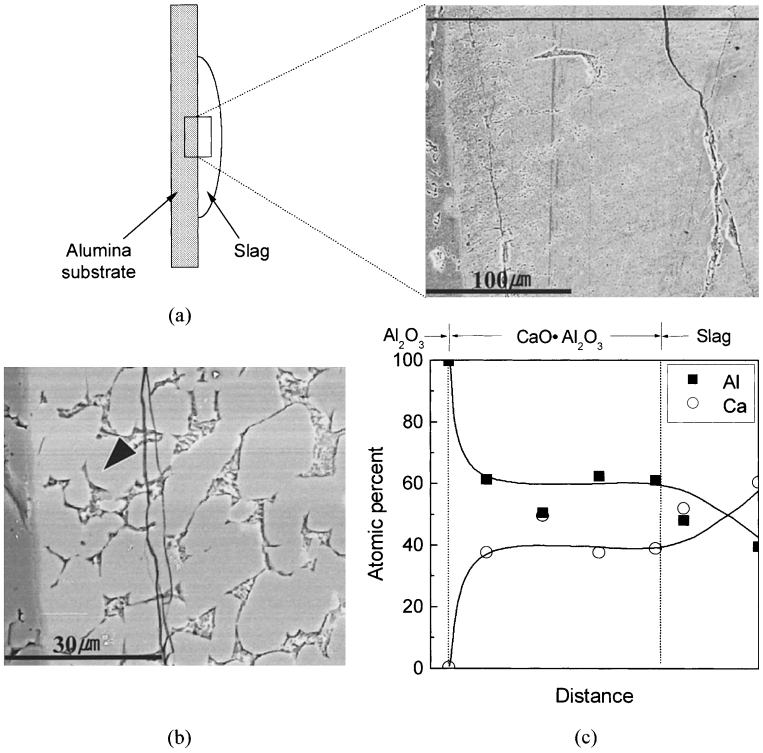

Fig. 5. Microscopic observation at the slag (A1)/alumina interface.
(a) Schematic representation of a quenched specimen, (b) SEM Image at the slag/alumina interface (▲: $CaO \cdot Al_2O_3$), (c) EPMA analysis.

1) The contact angle changes very rapidly in the first few seconds, followed by an asymptotic approach to an equilibrium value.
2) The rate of the change in the contact angle depends on the slag composition.
3) The equilibrium contact angle differs with different slag compositions.

A number of factors may be involved in governing the spreading behavior, *i.e.*, the change in the contact angle. These may include the slag viscosity, the surface and interfacial tension, and the surface roughness of the substrate. In addition, any chemical interaction between the slag and the substrate that may occur should also be taken into consideration.

3.2. Chemical Interactions at the Interface

In order to check if any chemical interactions took place at the interface, some specimens (slag+substrate) were rapidly taken out of the heating zone after the experiment and immediately quenched by blowing helium gas. The compositional change across the slag/substrate interface was investigated using electron probe microanalysis (EPMA). The result with the slag A1 (57.7%CaO–42.3% Al_2O_3) is given in **Fig. 5** where the compositional change across the interface is clearly visible. The alumina content in the slag phase increases towards the alumina substrate, but there is also a layer at which the composition stays constant. Considering the atomic percent ratio of Al/Ca being constant at about 2/1 at the layer as shown in Fig. 5, the phase which prevails at the layer should be the compound of $CaO \cdot Al_2O_3$. A similar study with different slag compositions has confirmed the formation of other compounds, *i.e.*, $CaO \cdot 2Al_2O_3$ with slag B1 and $CaO \cdot 6Al_2O_3$ with slag D4. With slags in a certain compositional range (*e.g.*, Slag E6) no compound formation was observed. In **Fig. 6** the results of the observation are represented together with the CaO–Al_2O_3–SiO_2 phase diagram. The formation of a compound layer may be explained by mutual interactions or reactions between the slag and alumina substrate. When molten slag comes into contact with the alumina substrate, alumina in the substrate dissolves into the slag and slag components diffuse into the alumina substrate. Slag composition in the vicinity of the interface continues to change in the direction toward the Al_2O_3 corner until the composition hits the primary field boundary of the corresponding compound. It is seen in Fig. 6 that in the case of slag B1 (59.4%CaO–5.0%SiO_2–35.5%Al_2O_3) the corresponding compound is $CaO \cdot 2Al_2O_3$ and the compound which actually forms is also $CaO \cdot 2Al_2O_3$. These observations tend to imply that the formation of a corresponding compound takes place at a relatively fast rate and the dissolution of alumina into the slag occurs in two steps: *i.e.*, formation of a CaO–Al_2O_3 compound and subsequent dissolution of the compound.

4. Discussion

4.1. Model Development for Spreading Behavior

As for the spreading of a liquid drop on a solid substrate, a number of models have been proposed, and some relevant to the present study are summarized in the following:

a) Model Proposed by Newman,[2] and Cherry–Holmes[3]

$$\cos\theta = \cos\theta_{e,app}(1 - ae^{-ct}) \quad \text{.....(1)}$$

where $a = 1 - \cos\theta_0/\cos\theta_e$, $c = \sigma_{LV}/\mu L$, $\cos\theta = (\sigma_{SV} - \sigma_{LS})/\sigma_{LV}$, θ_0 = contact angle at $t = 0$, $\theta_{e,app}$ = equilibrium contact

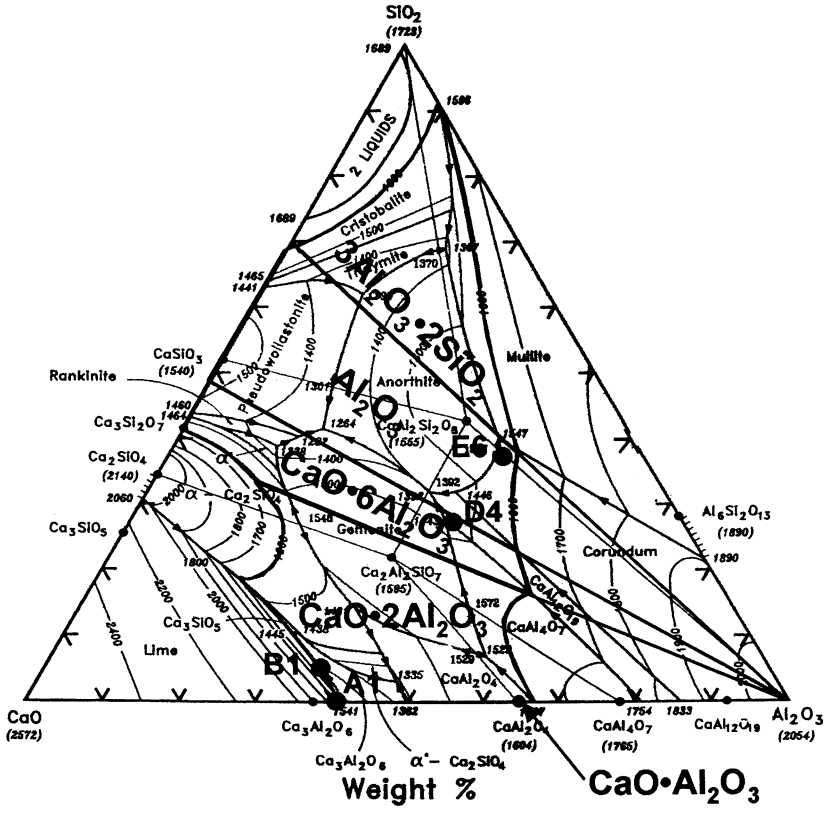

Fig. 6. The possible solid compound formation at the slag/alumina interface.[1)]

angle on a rough surface, θ=contact angle at t, μ=viscosity of the liquid drop, σ_{LV}=surface tension of the liquid drop, σ_{SV}=surface tension of the solid substrate, σ_{LS}=interfacial tension between the solid substrate and the liquid drop, L=scaling length.

b) Model Proposed by Ogarev *et al.*[4)]

$$t=\frac{\mu(3V_0/\pi)^{1/3}}{8\sigma_{LV}(\cos\theta_{e,app}-\cos\theta)\tan^{4/3}\theta} \quad \text{.....(2)}$$

where V_0=volume of the liquid drop.

c) Model Proposed by Schroeder[5)]

$$\cos\theta(t)=\cos\theta_0+\cos\theta_{e,app}[1-\exp(-mt^b)] \quad \text{.....(3)}$$

where m is related to surface tension and viscosity of liquid drop and b is related to the surface roughness of the solid substrate.

In order to confirm the validity of the above models for the present experimental geometry, a cold model experiment was carried out using liquid glycerol and a glass substrate. **Figure 7** shows experimental results together with predictions by the various models. It is seen that the Shroeder model results in excellent agreement with the experimental data, but either the Ogarev or Newman–Cherry–Holmes model does not show a good fit with the experimental results.

In order to apply the Schroeder model to the present liquid slag–alumina substrate system, the factor b in Eq. (3), which is related to the surface roughness of the substrate, must be determined in advance. The relationship between true roughness and the value b was examined through the cold model experiment using glycerol and glass substrates

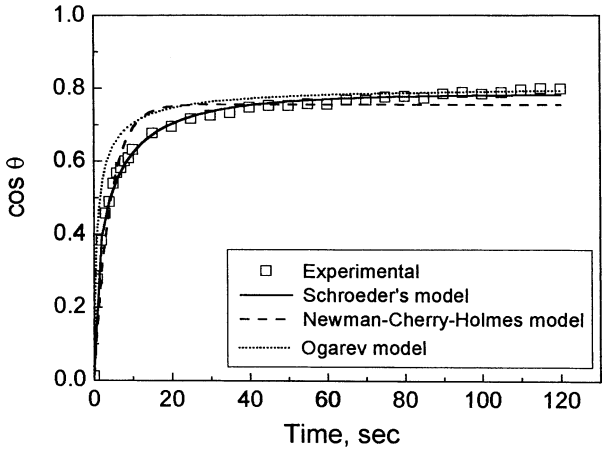

Fig. 7. Applications of various models to the spreading behavior of glycerol on glass.

of various surface roughness and the result is given in **Fig. 8**. Using this figure the value of b for the alumina substrate with surface roughness of R_a=0.553 μm was found to be 0.5675.

Taking zero time when the contact between the drop and substrate forms the right angle (t=0 at θ=90°), which leads to cos θ_0=0, the Schroeder model of Eq. (3) is simplified as,

$$\cos\theta(t)=\cos\theta_{e,app}[1-\exp(-mt^b)] \quad \text{.....(4)}$$

Applicability of the Schroeder model was examined by fitting Eq. (4) to each set of experimental results through regression analysis. Some of the results are given in **Fig. 9** and it is seen that the degree of agreement is unacceptably poor. It should be noted that the Schroeder model assumes

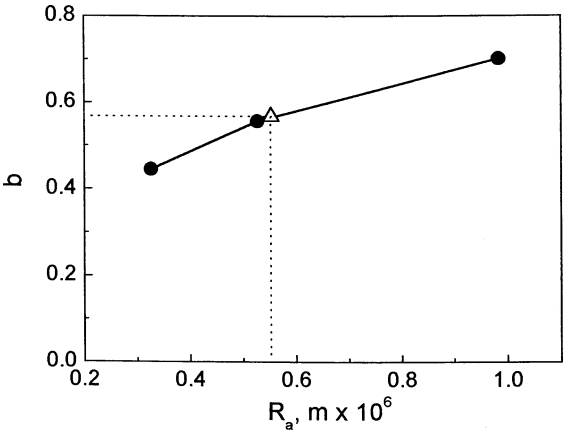

Fig. 8. Regression analysis of b for various surface roughnesses. (△: alumina substrate, ●: glass substrate)

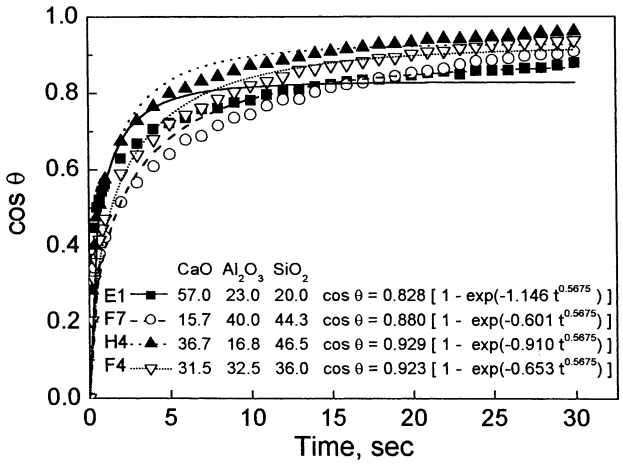

Fig. 9. Application of Schroeder's model to the spreading behavior of various slags (mass%) on an alumina substrate.

that the equilibrium contact angle ($\theta_{e,app}$) does not change with time but remains constant. In the present study, however, chemical interactions (dissolution and compound formation) take place at the interface and hence the equilibrium value of the contact angle should also change with time due to the compositional change at the interface. Therefore Eq. (4) needs to be modified to accommodate the change of $\theta_{e,app}$ with time. In order to express the equilibrium contact angle as a function of time, an assumption is now introduced; that is, the interfacial tension between slag and substrate varies exponentially with time. This assumption should not be considered unreasonable, since the compositional change due to mass transfer generally follows an exponential pattern with time and the interfacial tension is usually proportional to the materials compositions.[6] With this assumption, together with boundary conditions of $\theta=\theta^0_{e,app}$ at $t=0$, and $\theta=\theta^\infty_{e,app}$ at $t=\infty$, the following expression can be obtained:

$$\cos\theta_{e,app}(t) = [\cos\theta^\infty_{e,app} - (\cos\theta^\infty_{e,app} - \cos\theta^0_{e,app})\exp(-kt)] \quad \text{.....(5)}$$

where $\theta_{e,app}(t)$=equilibrium contact angle between slag and substrate at time t, $\theta^0_{e,app}$=equilibrium contact angle between the initial slag and alumina substrate, $\theta^\infty_{e,app}$=contact angle at $t=\infty$, and k=constant.

Combination of Eq. (5) and the original Shroeder model

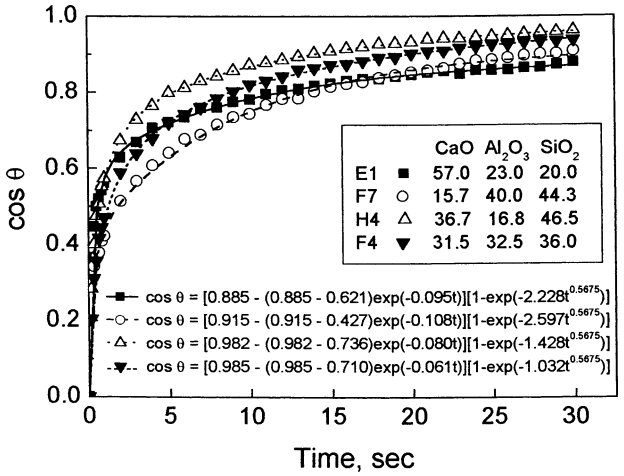

Fig. 10. Applications of the new model to the spreading behavior of various slags on an alumina substrate.

of Eq. (3) yields,

$$\cos\theta(t) = \cos\theta_0 + [\cos\theta^\infty_{e,app} - (\cos\theta^\infty_{e,app} - \cos\theta^0_{e,app})\exp(-kt)][1-\exp(-mt^b)] \quad \text{.....(6)}$$

Now, Eq. (6) was applied to the experimental results with different slag compositions, and the various terms ($\theta^0_{e,app}$, $\theta^\infty_{e,app}$, k, m) were determined through regression for each slag composition. **Figure 10** shows typical examples of the fitting of Eq. (6) to the experimental results. It is seen that the new model gives a striking agreement with the experimental results of the present study. The solid lines shown in Fig. 4 where experimental data are presented are in fact the results fitting with Eq. (6). These agreements prove that the new model of Eq. (6) correctly represents the spreading behavior of liquid slag on the alumina substrate. Application of the model enables us not only to describe the spreading behavior as a function of time, but also to determine $\theta^0_{e,app}$ which is the equilibrium contact angle to be formed between the alumina substrate and the slag if there were no chemical interactions at the interface. The various terms in Eq. (6), $\theta^0_{e,app}$, $\theta^\infty_{e,app}$, k, and m, which were determined for each slag composition by regression analysis are included in Table 1.

4.2. Effect of Surface Roughness

If the surface of a solid substrate is perfectly smooth, the adhesion tension (α) can be expressed as follows:

$$\alpha = \sigma_S - \sigma_{LS} = \sigma_L \cos\theta_{true} \quad \text{.....(7)}$$

where θ_{true} is the contact angle on a perfectly smooth surface.

If the surface roughness is considered, Eq. (7) needs to be modified as follows[7]:

$$r\alpha = r(\sigma_S - \sigma_{LS}) = \sigma_L \cos\theta_{app} \quad \text{.....(8)}$$

where θ_{app}=the contact angle on a rough surface, r= Wenzel's ratio ($=A/A_{app}$), A=the actual surface area between the liquid drop and substrate, and A_{app}=the apparent surface area between the liquid drop and substrate.

Combination of the above two equations yields,

$$\cos\theta_{app} = r\cos\theta_{true} \quad \text{.....(9)}$$

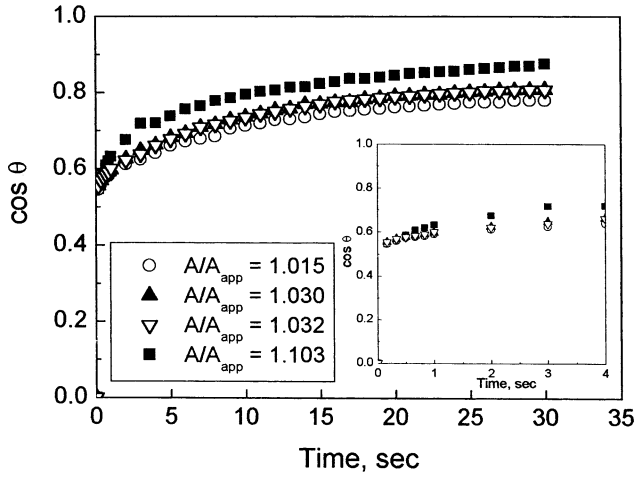

Fig. 11. Effect of surface roughness on spreading behaviors of C2 slag.
(54.7%CaO–11.6%SiO_2–33.7%Al_2O_3 in mass %)

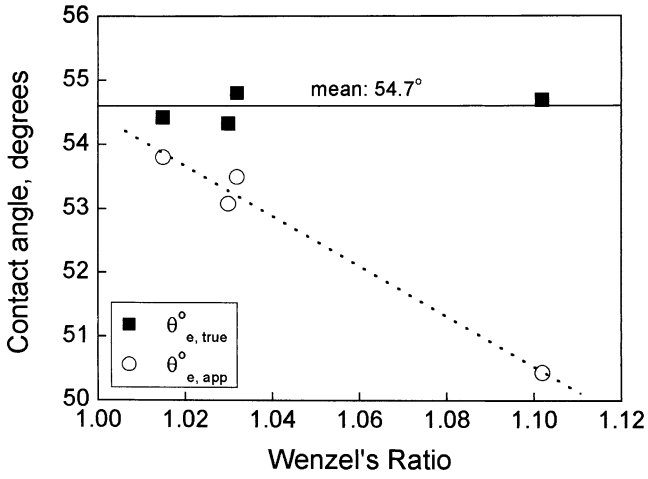

Fig. 12. Effect of surface roughness on the equilibrium contact angle.

It is noted from the above equation that if the true contact angle is less than 90°, then $\theta_{app} < \theta_{true}$, and the apparent contact angle decreases with increasing the roughness, whereas if the true contact angle is greater than 90°, the opposite is true. If the true contact angle is just 90°, the surface roughness will not exert any effect on the contact angle.

The Wenzel's ratio ($r=A/A_{app}$) can be evaluated using the following relationship:

$$\frac{A}{A_{app}} = \left(\frac{l}{l_0}\right)^2 \quad \text{.....(10)}$$

where l and l_0 are the actual profile length and the apparent length, respectively.

The actual profile length can be measured by tracing the actual contour of the surface. In the present study the actual profile length was measured using a non-contacting surface roughness measuring apparatus (Rodenstock RM600®). The measured profile length ratios are represented in Table 2, together with the calculated Wenzel's ratios.

The effect of the surface roughness was examined using Slag C2 (54.7%CaO–33.7%Al_2O_3–11.6%SiO_2) and the results are summarized in **Fig. 11**.

In Fig. 11, it is seen that the spreading behavior differs with different surface roughness, and hence different values of the apparent equilibrium contact angle ($\theta^0_{e,app}$) result. However, the true equilibrium contact angles ($\theta^0_{e,true}$) calculated using Eq. (9) are very much the same for the different surface roughness (see **Fig. 12**).

4.3. Equilibrium Contact Angles

In order to obtain the true equilibrium contact angle ($\theta^0_{e,true}$) for all slag compositions examined in the present study, the Wenzel's equation of Eq. (9) should be applied to the values of $\theta^0_{e,app}$ in Table 1 since the values of $\theta^0_{e,app}$ in Table 1 obtained by fitting the spreading model of Eq. (6) to the experimental data contains the surface roughness. The true equilibrium contact angles so obtained are presented in **Fig. 13**. Iso-angle lines are also constructed in the figure. It is seen that the equilibrium contact angle varies with slag composition to a large extent. Several important trends can

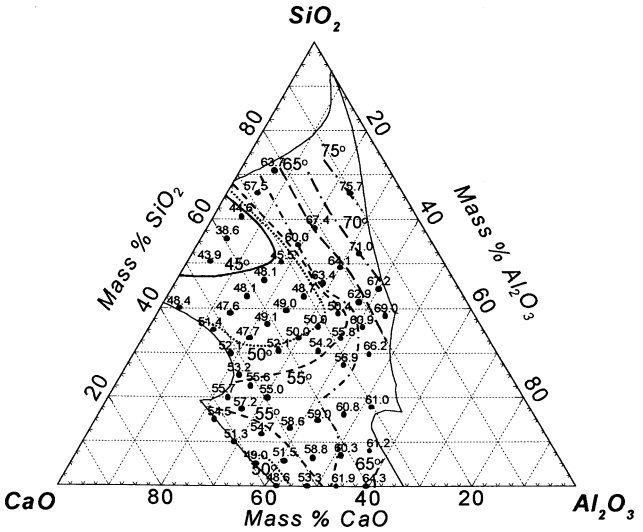

Fig. 13. True contact angles between CaO–SiO_2–Al_2O_3 slag and alumina at 1 873 K.

be identified from Fig. 13:

1) In the region of low SiO_2 content, the slag with higher CaO content exhibits a smaller contact angle, *i.e.*, better wettability with alumina.
2) For the slag with a given CaO/SiO_2 ratio, an increase in Al_2O_3 results in an increase in the contact angle, *i.e.*, decrease in wettability.
3) For a given CaO/Al_2O_3 ratio, the variation of the contact angle with SiO_2 content shows a minimum.

In order to determine factors governing the equilibrium contact angle, it is attempted to compare the variation of the contact angle with that of the interfacial tension of the system of liquid CaO–Al_2O_3–SiO_2/solid Al_2O_3 at 1 873 K. However, there is no report on the interfacial tension of the above system, and hence it was evaluated by using the Young's equation:

$$\cos\theta_{SI} = \frac{\sigma_I - \sigma_{SI}}{\sigma_S} \quad \text{.....(11)}$$

where θ_{SI} is the contact angle between the slag and substrate,

The interfacial tension between the slag and the alumina

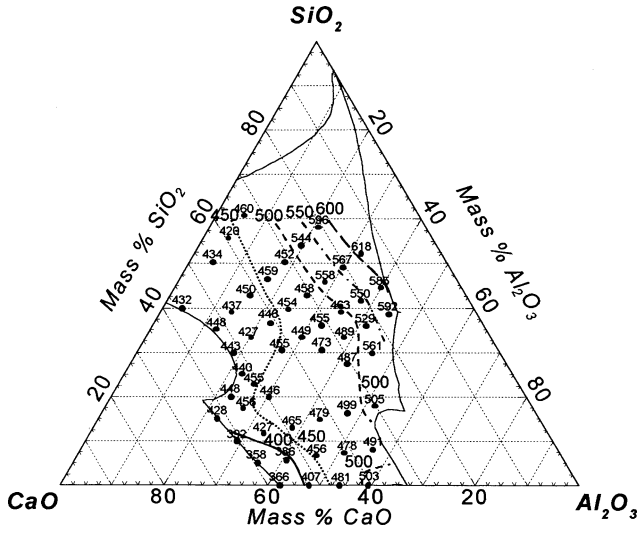

Fig. 14. Interfacial tension ($\times 10^{-3}$ N m^{-1}) between CaO–SiO_2–Al_2O_3 slag and Al_2O_3.

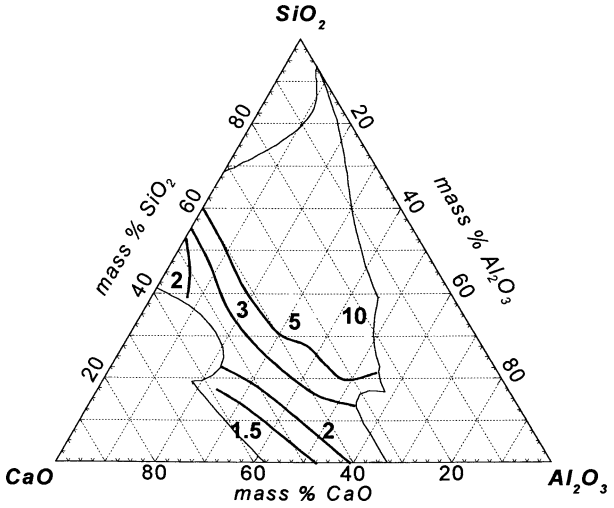

Fig. 15. Viscosities (poise) of CaO–SiO_2–Al_2O_3 slag system at 1 873 K.[10]

substrate (σ_{SI}) can be calculated using the above equation, provided that the equilibrium contact angle (θ_{SI}), the surface tensions of the alumina substrate (σ_I) and the slag (σ_S) be known. These values can readily be obtained: σ_{SI} has already been determined in the present study (see Fig. 13), σ_I by applying Nakajima's suggestion,[8] and by employing the model developed by the present authors.[9] **Figure 14** shows the result of evaluation of the interfacial tension between the liquid CaO–Al_2O_3–SiO_2 slag and the solid Al_2O_3 at 1 873 K. Upon comparison of Fig. 13 with Fig. 14, it can immediately be noticed that the equilibrium contact angle is closely related to the interfacial tension; *i.e.*, the higher the interfacial tension, the larger the contact angle.

Figure 15 shows the iso-viscosity diagram of the CaO–Al_2O_3–SiO_2 system at 1 873 K.[10] This diagram shows that a basic property which governs the viscosity may exert a certain degree of influence on the equilibrium contact angle, but it is not the major factor.

Table 2. Measurement data of the profile length ratio for various substrates.

l_r	1.0077	1.0150	1.0159	1.0501
Wenzel's ratio	1.015	1.030	1.032	1.103

In summary, it can now be concluded that interfacial tension is the major factor which governs the equilibrium contact angle, *i.e.*, the wettability.

5. Conclusions

The wetting behavior of molten CaO–Al_2O_3–SiO_2 with solid Al_2O_3 was investigated at 1 873 K using the sessile drop method in which a liquid slag drop was allowed to spread on an alumina substrate. A new model was developed which successfully represents the time dependence of the contact angle, in other words, the spreading behavior, of a liquid drop on a solid substrate. The model takes into consideration chemical interactions which continually take place at the interface between the solid Al_2O_3 and molten CaO–Al_2O_3–SiO_2. From the experimental results and the model the equilibrium contact angle was determined for a number of different slag compositions, with which an iso-contact angle diagram was constructed. The following are a summary of the findings:

(1) Interfacial tension was the major factor governing the equilibrium contact angle.

(2) In the region of low SiO_2 content, the slag with higher CaO content exhibits smaller contact angle, *i.e.*, better wettability with alumina.

(3) For the slag with a given CaO/SiO_2 ratio, an increase in Al_2O_3 results in an increase in the contact angle, *i.e.*, decrease in wettability.

(4) For a given CaO/Al_2O_3 ratio, the variation of the contact angle with SiO_2 content shows a minimum.

(5) The contact angle decreases with increasing the surface roughness of the alumina substrate.

Acknowledgement

The authors greatly appreciate the financial support of POSCO for the present study.

REFERENCES

1) G. Eriksson and A. D. Pelton: *Metall. Trans. B*, **24** (1993), 807.
2) S. Newman: *J. Colloid Interface Sci.*, **26** (1968), 209.
3) B. W. Cherry and C. M. Holmes: *J. Colloid Interface Sci.*, **29** (1969), 174.
4) V. A. Ogarev, T. N. Timonina, V. V. Arslanov and A. A. Trapeznikov: *J. Adhesion*, **6** (1974), 337.
5) L. W. Schroeder: Contact Angle, Wettability and Adhesion, (1993), 349.
6) K. Nakajima: *Tetsu-to-Hagané*, **80** (1994), 383.
7) R. N. Wenzel: *Ind. Eng. Chem.*, **28** (1936), 988.
8) K. Nakajima: *Tetsu-to-Hagané*, **80** (1994), 599.
9) J. Y. Choi and H. G. Lee: *ISIJ Int.*, **42** (2002), 221.
10) S. Seetharaman and D. Sichen: *ISIJ Int.*, **37** (1997), 109.